Dynamical Self-Assembly of Nanocrystal Superlattices during Colloidal Droplet Evaporation by *in situ* Small Angle X-Ray Scattering

Suresh Narayanan and Jin Wang
Advanced Photon Source, Argonne National Laboratory, Argonne, Illinois 60439, USA

Xiao-Min Lin
Materials Science Division, Chemistry Division and Center for Nanoscale Materials, Argonne National Laboratory, Argonne, Illinois 60439, USA

(Received 16 March 2004; published 24 September 2004)

The nucleation and growth kinetics of highly ordered gold nanocrystal superlattices during the evaporation of nanocrystal colloidal droplets was elucidated by *in situ* time-resolved small-angle x-ray scattering. We demonstrated for the first time that the evaporation rate can affect the dimensionality of the superlattices. The formation of two-dimensional nanocrystal superlattices at the liquid-air interface of the droplet has exponential growth kinetics that originates from interface crushing.

DOI: 10.1103/PhysRevLett.93.135503 PACS numbers: 61.46.+w, 78.67.Bf, 78.70.Ck, 81.16.Dn

The microscopic mechanism for self-organization of ligand-stabilized nanocrystals has been well established [1,2]. The interparticle van der Waals interaction provides the attractive force to induce the self-assembly, whereas the steric interaction due to the ligand interdigitation provides the balancing force to create stable structures. However, the macroscopic patterns created by such interactions vary dramatically under different conditions. Even for a simple case of evaporating a colloidal droplet of nanocrystals on a surface, a variety of patterns has been reported, ranging from ordered two-dimensional (2D), three-dimensional (3D) nanocrystal superlattices (NCSs) [3–5], and fractal-like aggregates [6,7] to percolated networks [8–10]. A common notion is that the self-assembling process occurs at the liquid-substrate interface [11], where the competing effects from the diffusion of nanocrystals along the substrate and solvent dewetting could lead to pattern formation far away from equilibrium [12]. Having such vastly different structures of nanocrystal assembly hinders the exploration of their physical properties [3,13,14], as well as creating obstacles for device applications [11,15]. It is therefore essential to further understand and control the nanocrystal self-assembly mechanism.

Recently, highly ordered 2D gold NCSs with domain size up to tens of microns were demonstrated by evaporating a nanocrystal colloidal droplet with the presence of an excess amount of dodecanethiol ligand molecules [5]. Figure 1(a) shows a transmission electron microscopy (TEM) image of a region of a resulting highly ordered NCS. The high degree of ordering and large domain size indicates the formation of NCSs most likely occurs through nucleation and growth. It is difficult to explain the high crystallinity of the superlattices if the self-assembly occurs on the substrate at the last instance when the solvent dewets the surface. In this Letter, we report an *in situ,* nonintrusive, small-angle x-ray scattering (SAXS) measurement to elucidate the formation of gold NCSs as the colloidal droplet evaporates. Contrary to the previous notion, these highly ordered 2D superlattices are formed at the liquid-air interface of the liquid droplet during the solvent evaporation. Changing the solvent evaporation rate can lead to either 2D or 3D NCS formation using the same colloidal nanocrystals.

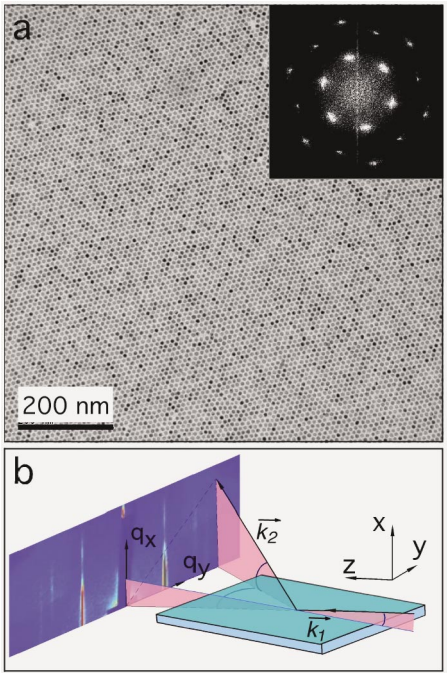

FIG. 1 (color). Characterization of 2D nanocrystal superlattices formed by colloidal droplet evaporation: (a) TEM image of a highly ordered gold nanocrystal monolayer. The inset shows Fourier transformation of the superlattice and (b) schematic diagram of the scattering geometry used for the *in situ* SAXS measurement. Incident x rays are along the z direction. The substrate is initially aligned in the y-z plane, then tilted 0.3° relative to the incident x rays.

We used monodispersed dodecanethiol ligated gold nanocrystals with an average diameter of 7.5 and 5.8 nm in two different experimental runs [16,17], and with the particle number concentration adjusted to be approximately 10^{13} mL^{-1}, just enough to form a monolayer. The volume concentration of thiol was 0.63%. The SAXS experiments were conducted at the 1-BM beam line of the Advanced Photon Source (APS). A colloidal solution of 10 μl was deposited onto a rectangular silicon nitride substrate (3×4 mm^2). The incident synchrotron x-ray beam was monochromatized to 8.0 keV by a double-crystal monochromator while two sets of horizontal (H) and vertical (V) slits were used to define the beam size to 0.2 (H) $\times$ 0.2 (V) mm^2. We chose a laboratory coordinate system as shown in Fig. 1(b) so that the incident x-ray beam is along the z direction and the substrate surface is in the y-z plane. The samples were initially aligned using the substrate as a reference; thus the top surface of the substrate was centered in the x-ray beam along the x direction. The substrate was then titled 0.3° relative to the incident beam. The scattered x rays passed through a helium flight path and were collected by either an image plate or a charge-coupled device detector.

The dynamical self-assembling process can be observed by positioning the incident beam at the bottom center of the droplet to accommodate the changing meniscus of the droplet as it evaporates. Figure 2 shows a typical time evolution of the SAXS patterns after the droplet is deposited on the substrate. The droplet is evaporated in air at room temperature (23 °C) with the mass of the droplet decreasing approximately at 0.66 mg/min. The initial thickness of the droplet is typically more than 2 mm. No visible scattering pattern is observed in the first 2 min, which indicates that there are no ordered superstructures initially in the droplet [Fig. 2(a)]. After that, an elliptically shaped diffraction ring is observed [Fig. 2(b)]. The section of the scattering ring near $q_y = 0$ gradually becomes more diffuse in the q_x direction and eventually disappears, while the intensity of the scattering corresponding to the in-plane long-range order increases dramatically [Figs. 2(c) and 2(d)]. The scattering pattern in Fig. 2(d) remains unchanged for hours during which a thin liquid film, less than 100 μm in thickness, with a high concentration of dodecanethiol remains on the substrate surface. To illustrate the kinetics of the nanocrystal array growth, Fig. 2(e) shows the experimental time evolution of the intensity of the (10) powder-diffraction peak at $q_x = 0$, plotted in a seminatural log format. The intensity increases exponentially with time before becoming saturated after 8 min (data not shown). When the liquid film is completely dried and the NCSs are deposited on the substrate, the downward scattering is suppressed by absorption and total external reflection of the substrate [18]. In contrast, the scattering patterns after 8 min [Fig. 2(d)] are considerably more symmetric in the vertical direction (q_x), indicating the 2D NCSs form

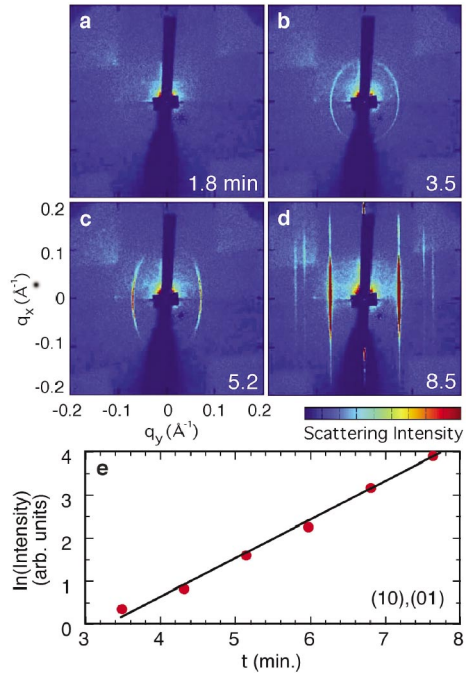

FIG. 2 (color). (a)–(d) *In situ* SAXS patterns of 2D gold NCSs formation during the evaporation of a 10 μl droplet with a particle density of 10^{13} mL^{-1}. The evaporation rate is approximately 0.66 mg/min. Time in unit of minutes is in reference to the deposition of colloid droplet. The average diameter of the nanocrystals is 7.5 nm determined by TEM. The cross-bar feature is the shadow image of the beam stop. (e) Time evolution of the normalized scattering intensity of the monolayer (10) powder diffraction, with an exponential fit.

at the liquid-air interface and are elevated above the substrate. In both cases, the scattering occurs close to the grazing incident small-angle x-ray scattering condition [19–21], because the monolayer is almost parallel to the substrate. Considering the geometry of our experimental setup, symmetrical scattering patterns such as shown in Fig. 2(d) can be obtained only when the monolayer is at least 49 μm above the substrate. The self-assembly of nanocrystals at the liquid-air interface was further confirmed by using a wider x-ray beam measured to be 1.5 (H) $\times$ 0.2 (V) mm^2, positioned near the edge of the droplet [22]. Bragg diffraction patterns from the 2D NCSs were observed rotating along with the x-ray reflection from the meniscus surface as the droplet flattens due to evaporation. We should emphasize that, unlike experiments carried out on the Langmuir trough [23], no aqueous subphase was used in our experiments. Both the nanocrystal ligand chain and the toluene solvent are hydrophobic in nature.

A comprehensive understanding of the formation of the 2D gold NCS monolayer can be achieved by comparing the simulated SAXS patterns during the evaporation process with the experimental data. The initial elliptically shaped x-ray scattering pattern, as well as its evolution, can be modeled by the "powder" diffraction of 2D superlattice domains with varying x-ray incident angles. As

shown in the schematic cross-section diagram in Fig. 3(a), the x-ray incident angle α at the liquid-air interface varies during the droplet evaporation, while the edges of the droplet are pinned by the substrate. The reciprocal lattice of a 2D crystal is infinitely long rods arranged in a 2D form. The constructive interference occurs when the in-plane component of the scattering vector satisfies the Bragg condition, which can happen at any incident angle [24]. To model this, we define a sample coordinate system (x', y') that is attached to the lattice plane as shown in Fig. 3(a). In a kinematical approach of x-ray diffraction [25], the averaged powder-diffraction intensity from many 2D lattice domains in the reciprocal space is distributed in a circular ring defined by $\sqrt{q_{x'}^2 + q_{y'}^2} = |\mathbf{q}_{h,k}|$, where $(q_{x'}, q_{y'})$ are the momentum transfer (MT) components in the sample coordinates that satisfy the Bragg diffraction condition defined by the scattering vector $\mathbf{q}_{h,k}$. The scattering patterns recorded by the 2D detectors in the laboratory coordinate are related to the circular powder ring in the sample coordinate by a linear transformation. Therefore the Bragg scattering condition in the laboratory coordinate is described approximately by $\sqrt{(q_x \sin\alpha)^2 + q_y^2} = |\mathbf{q}_{h,k}|$, where (q_x, q_y) are the MT components in laboratory coordinate. The short axis of the ellipse is in the q_y direction and has a magnitude of $|\mathbf{q}_{h,k}|$, whereas the long axis is in the q_x direction and has a magnitude of $|\mathbf{q}_{h,k}|/\sin\alpha$. For example, the elliptical scattering pattern in Fig. 2(b) indicates, at 3.5 min into the evaporation process, the 2D NCSs formed at the interface, which is orientated about 52.4° with respect to the incoming x-ray beam. The complete scattering intensity is the product of the lattice structure factor and the form factor of a spherical nanocrystal expressed as $|F(q)|^2 = [\frac{3[\sin(qr) - qr\cos(qr)]}{(qr)^3}]^2$, where $q = \sqrt{q_x^2 + q_y^2 + q_z^2}$, and r is the radius of the sphere. As the liquid droplet evaporates, the scattering geometry approaches a grazing incidence angle with respect to the sample ($\alpha = 0.3°$). In this case, the scattering intensity distribution along the q_y direction corresponds to the structure factor of the in-plane lattice and that along q_x reveals the form factor of the individual nanocrystal. Figures 3(b)–3(e) show the simulation results at different stages of evaporation, based on a 2D hexagonal close-packed NCS with an average diameter of 7.5 nm (polydispersity of 7%) and a 10.3 nm center-to-center spacing. The x-ray scattering intensity data [Fig. 2(e)] are found to be proportional to the integrated intensity after being normalized by the changing x-ray footprint size on the sample due to the variation of the x-ray incident angle.

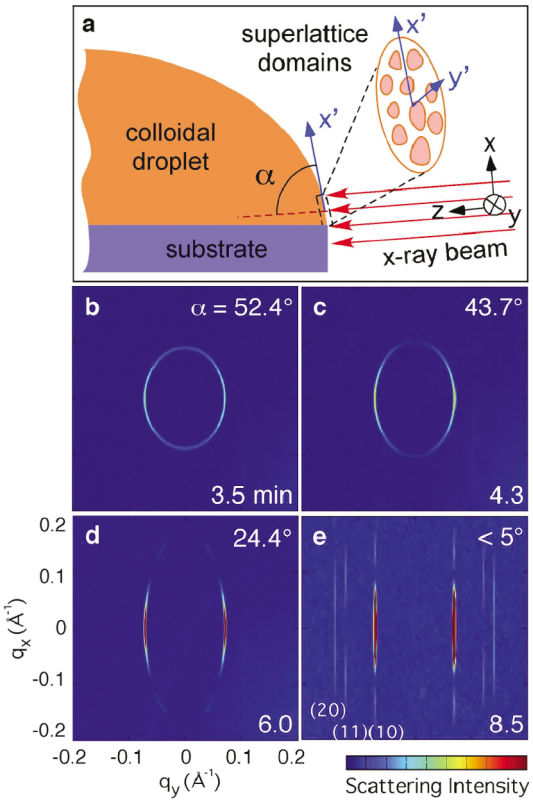

FIG. 3 (color). (a) Schematic cross sectional diagram of the x-ray beam and the colloidal droplet. (b)–(e) Simulation results based on a monolayer of 2D domains oriented at an angle α with respect to the incident x-ray beam at the liquid-air interface. The time in each frame corresponds to the real time used in the experiments.

The formation of the 2D gold NCSs can be understood using a kinetic "crushing" model proposed by Nguyen and Witten [26]. The diffusion constant (D) of the nanocrystals with a hydrodynamic radius R (5.1 nm) can be estimated using the Stokes-Einstein relation ($D = k_B T/6\pi\eta R$) and the viscosity of dodecanethiol ($\eta = 2.98cp$), assuming that toluene completely evaporates near the liquid-air interface. Since the major change in scattering patterns occurs at a time scale of 1 min, we can compare the diffusion distance of nanocrystals in 1 min with the change of the liquid-air interface during the same time interval. Under a random walk model, the average distance a nanocrystal can diffuse within 1 min is $\sqrt{\langle r^2 \rangle} = \sqrt{6Dt} \approx 70\ \mu$m. Since the air-liquid interface decreases faster than 70 μm/min during initial evaporation, as measured by monitoring the thickness change of the droplet in real time, nanocrystals will accumulate at the 2D liquid-air interface and eventually induce 2D crystallization.

The exponential increase of the scattering intensity [Fig. 2(e)] also supports the interface crushing model, in contrast to the power-law behavior in the 2D diffusion coarsening mechanism [27]. In the crushing case, domain growth mainly occurs through incorporating nanocrystals impinging the domain surface from below when it collapses with the evaporating liquid-air interface. The growth rate of a domain with size S is $dS/dt \sim nS\upsilon$, where n is the density of the nanocrystal and υ is the collapsing rate. We note n and υ are approximately constant during most of the evaporation. The crushing effect

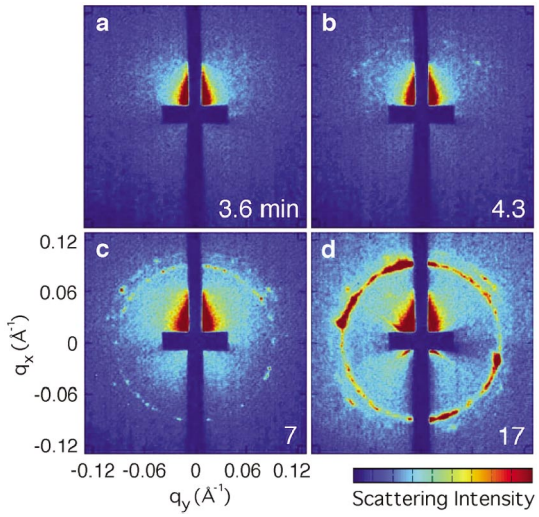

FIG. 4 (color). *In situ* x-ray scattering patterns during the evaporation of a 10 μl gold nanocrystal colloidal droplet with a particle density of 10^{13} mL^{-1} and evaporation rate of 0.22 mg/min. The average diameter of the nanocrystals is 5.8 nm.

thus leads to an exponential growth of domain size, which is a much more dominant process than the power-law growth by 2D diffusion at the interface.

One prediction of this kinetic crushing model is that the formation of the 2D NCSs should be affected by the evaporation rate. A slower initial evaporation rate could allow the nanocrystals to diffuse away from the interfacial layer before the concentration reaches its critical value for 2D crystallization. The formation of 3D superlattices will then occur in the bulk of the droplet. Figure 4 shows the time evolution of scattering patterns when the droplet is evaporated at approximately 0.22 mg/min. Indeed, 3D superlattices form and persist during the entire evaporation process. Using the same gold colloidal solution, but with different evaporation rates, both the 2D NCSs and 3D NCSs formation can be reproduced consistently.

In summary, this study shows the kinetics of evaporation strongly affect the structure of NCS formation. With a slight excess of thiol in the solution, 2D gold NCSs can form exponentially at the liquid-air interface when the evaporation is fast enough to induce nanocrystal accumulation at the interface, whereas under a much slower evaporation condition, nanocrystals can diffuse away from the interface and form 3D gold NCSs inside the droplet. Exploring this kinetics-driven self-assembling process using real-time x-ray scattering techniques should enable us to better control the organization of nanoscale building blocks and to study phenomena such as particle and domain dynamics and order-to-disorder phase transition.

We thank T. T. Nguyen, T. A. Witten, T. P. Bigioni, H. M. Jaeger, and C. M. Sorensen for extensive discussions. This work and use of APS are supported by the U.S. Department of Energy (DOE), BES-Materials Sciences, under Contract No. W-31-109-ENG-38, by DOE Center for Nanoscale Materials, and by the University of Chicago–Argonne National Laboratory Consortium for Nanoscience Research (CNR).

[1] P. C. Ohara *et al.*, Phys. Rev. Lett., **75**, 3466 (1995).
[2] Z. L. Wang *et al.*, J. Phys. Chem. B **102**, 3068 (1998).
[3] C. B. Murray, C. R. Kagan, and M. G. Bawendi, Science **270**, 1335 (1995).
[4] L. Motte *et al.*, J. Phys. Chem. B **101**, 138 (1997).
[5] X. M. Lin *et al.*, J. Phys. Chem. B **105**, 3353 (2001).
[6] G. Ge and L. Brus, J. Phys. Chem. B **104**, 9573 (2000).
[7] J. Tang, G. Ge, and L. E. Brus, J. Phys. Chem. B **106**, 5653 (2002).
[8] C. Stowell and B. A. Korgel, Nano Lett. **1**, 595 (2001).
[9] M. Maillard *et al.*, J. Phys. Chem. B **104**, 11871 (2000).
[10] P. Moriarty, M. D. R. Taylor, and M. Brust, Phys. Rev. Lett., **89**, 248303 (2002).
[11] C. B. Murray *et al.*, IBM J. Res. Dev. **45**, 47 (2001).
[12] E. Rabani *et al.*, Nature (London) **426**, 271 (2003).
[13] F. Remacle *et al.*, J. Phys. Chem. B **102**, 7727 (1998).
[14] R. Parthasarathy, X. M. Lin, and H. M. Jaeger, Phys. Rev. Lett., **87**, 186807 (2001).
[15] D. Weller and A. Moser, IEEE Trans. Magn. **35**, 4423 (1999).
[16] X. M. Lin, C. M. Sorensen, and K. J. Klabunde, J. Nanopart. Res. **2**, 157 (2000).
[17] S. Stoeva *et al.*, J. Am. Chem. Soc. **124**, 2305 (2002).
[18] See EPAPS Document No. E-PRLTAO-93-051438 for a movie of *in situ* scattering patterns of 2D nanocrystal superlattice formation during the evaporation of a colloidal droplet. A direct link to this document may be found in the online article's HTML reference section. The document may also be reached via the EPAPS homepage (http://www.aip.org/pubservs/epaps.html) or from ftp.aip.org in the directory /epaps/. See the EPAPS homepage for more information.
[19] G. Renaud *et al.*, Science **300**, 1416 (2003).
[20] A. Gibaud *et al.*, Europhys. Lett. **63**, 833 (2003).
[21] D.-M. Smilgies *et al.*, Synchrotron Radiation News **15**, 35 (2002).
[22] See EPAPS Document No. E-PRLTAO-93-051438 for an *in situ* measurement using a wide x-ray beam positioned near the edge of the droplet. A direct link to this document may be found in the online article's HTML reference section. The document may also be reached via the EPAPS homepage (http://www.aip.org/pubservs/epaps.html) or from ftp.aip.org in the directory /epaps/. See the EPAPS homepage for more information.
[23] R. P. Sear *et al.*, Phys. Rev. E **59**, R6255 (1999).
[24] See EPAPS Document No. E-PRLTAO-93-051438 for Bragg scattering from a 2D lattice. A direct link to this document may be found in the online article's HTML reference section. The document may also be reached via the EPAPS homepage (http://www.aip.org/pubservs/epaps.html) or from ftp.aip.org in the directory /epaps/. See the EPAPS homepage for more information.
[25] B. E. Warren, *X-Ray Diffraction* (Dover Publications, New York, 1990).
[26] T. T. Nguyen and T. A. Witten (to be published).
[27] A. Lo and R. T. Skodje, J. Chem. Phys. **112**, 1966 (2000).